Self-fluorescent Antibiotic MoO_x-Hydroxyapatite: A Nano-theranostic Platform for Bone Infection Therapies

Damián Placente [a], *Juan. M. Ruso* [b], *Mónica Baldini* [c], *Juan M. Sieben* [e§] *Juan A. Laiuppa* [c,d§], *Graciela E. Santillán* [c,d], *Paula V. Messina* [a]*

(a) INQUISUR – CONICET, Department of Chemistry, Universidad Nacional del Sur, B8000CPB, Bahía Blanca, Argentina. (b) Soft Matter and Molecular Biophysics Group, Department of Applied Physics, University of Santiago de Compostela, 15782 Santiago de Compostela, Spain (c) Department of Biology, Biochemistry and Pharmacy, Universidad Nacional del Sur, B8000ICN, Bahía Blanca, Argentina. (d) INBIOSUR – CONICET. (e) INIEC – CONICET, Department of Chemistry Engineering, Universidad Nacional del Sur, B8000CPB Bahía Blanca, Argentina

* Author to whom correspondence should be addressed. Tel: +54 291 4595159. Fax: +54 291 4595160. Electronic mail: pmessina@uns.edu.ar.

§ Juan M. Sieben and Juan A. Laiuppa have contributed equally to this work.

ESI-1 Direct unit cell crystallographic parameters and crystalline phase fraction

Diffraction patterns of all samples were equivalent to the hexagonal crystal form of HA ($P6_3/m$ space group symmetry, a = b ≠ c; α = β = 90º; γ = 120°) and the tetragonal crystal form of powellite (I41/a space group symmetry, a = b ≠ c; α = β = γ = 90º). The lattice geometry parameters (*a, b, c)* and the volume of the direct unit cell *(V),* were computed by Rietveld refinement using the Rietica v4.2 software package [1] on basis of the following equation: [2]

Hexagonal system

$$\frac{1}{(d_{hkl})^2} = \left[{}^4/_3\right]\left[(h^2 + hk + k^2)/a^2\right] + \left[l^2/c^2\right] \quad (1)$$

$$V = \left[{}^{\sqrt{3}}/_2\right]\left[a^2 c\right] \quad (2)$$

Tetragonal system

$$\frac{1}{(d_{hkl})^2} = \left[(h^2 + k^2)/a^2\right] + \left[l^2/c^2\right] \quad (3)$$

$$V = a^2 c \quad (4)$$

where, d_{hkl} is the interplanar distance computed by the Bragg equation ($\lambda = 2d_{hkl}\, sen\, \theta$) and (*hkl*) are the Miller index of the symmetric reflections used in the calculus.[2]

The fraction of HA crystalline phase ($X_{c,HA}$) in all samples was evaluated using the following equation: [3]

$$X_{c,HA} = 1 - \frac{v_{112/300}}{I_{300}} \quad (5)$$

where I_{300} is the intensity of (300) Miller plane family diffraction peak and $\upsilon_{112/300}$ is the intensity of the hollow between (112) and (300) HA diffraction peaks. Verification was done with the relation:[4]

$$B_{002}\sqrt[3]{X_{c,HA}} = K \quad (6)$$

where *K* is a constant found equal to 0.24 for a very large number of different HA powders, [5] and B_{002} is the full-width at the half-maximum (FWHM) in degrees of the (002) reflection. The expected uncertainties are around 15 %.

ESI-2 Molecular modeling

Atomic coordinates and isotropic displacement parameters (in Å ^{2}):

Table ESI1. Stoichiometric HA crystallographic unit cell: $(Ca^{+2})_{10}(PO_4^{-3})_6(OH^-)_2$

Atom	Ox.	Wyck.	x	y	z	B
Ca1	+2	4f	2/3	1/3	0.01030	1.3000
Ca2	+2	6h	0.24627	0.23737	1/4	1.3000
P1	+3	6h	0.02886	0.40568	1/4	1.3000
O1	-2	12i	0.07903	0.34479	0.05933	1.3000
O2	-2	6h	0.49079	0.15330	1/4	1.3000
O3	-2	6h	0.12872	0.59834	1/4	1.3000
O4	-2	2a	0	0	1/4	1.3000

Table ESI2. Non-stoichiometric HA crystallographic unit cell:

$(Ca^{+2})_{9.12}(PO_4^{-3})_{5.12}(HPO_4^{-2})_{0.88}(OH^-)_{1.12}$

Atom	Ox.	Wyck.	x	y	z	B
Ca1	+2	4f	2/3	1/3	0.03349	0.1000
Ca2	+2	6h	0.02512	0.25931	1/4	0.1000
P1	+5	6h	0.65133	0.01663	1/4	0.1000
O1	-2	12i	0.38037	0.25707	0.05284	0.1000
O2	-2	6h	0.28291	0.43395	1/4	0.1000
O3	-2	6h	0.51982	0.08994	1/4	0.1000
O4	-2	2a	0	0	1/4	0.1000

Table ESI3. Stoichiometric Powellite crystallographic unit cell: $(Ca^{+2})(MoO_4^{-2})$

Atom	Ox.	Wyck.	x	y	z
Ca1	+2	4a	0	3/4	7/8
Mo1	+5	4b	0	3/4	3/8
O1	-2	16f	0.35077	0.02671	0.79736

Table ESI4. HA crystallographic unit cell in material HA/MoO (II), similar results were obtained for HA/MoO (I).

Atom	Ox.	Wyck.	x	y	z	B
Ca1	+2	4f	2/3	1/3	0.01973	0.1000
Ca2	+2	6h	0.01898	0.26374	1/4	0.1000
P1	+5	6h	0.63685	0.02386	1/4	0.1000
O1	-2	12i	0.36017	0.25386	0.06333	0.1000
O2	-2	6h	0.26039	0.42790	1/4	0.1000
O3	-2	6h	0.55239	0.11574	1/4	0.1000
O4	-2	2a	0	0	1/4	0.1000

Table ESI5. HA crystallographic unit cell in material HA/MoO (III)

Atom	Ox.	Wyck.	x	y	z	B
Ca1	+2	4f	2/3	1/3	0.00695	0.1000
Ca2	+2	6h	0.06071	0.28164	1/4	0.1000
P1	+5	6h	0.65470	0.03798	1/4	0.1000
O1	-2	6h	0.51574	0.04298	1/4	0.1000
O2	-2	6h	0.24860	0.48007	1/4	0.1000
O3	-2	12i	0.34177	0.26202	0.07495	0.1000
O4	-2	2a	0	0	1/4	0.1000

Table ESI6. HA crystallographic unit cell in material HA/MoO (IV)

Atom	Ox.	Wyck.	x	y	z	B
Ca1	+2	4f	2/3	1/3	0.04990	0.0000
Ca2	+2	6h	0.05502	0.24312	1/4	0.0000
P1	+5	6h	0.58762	0.01491	1/4	0.0000
O1	-2	12i	0.32273	0.42483	0.07595	0.0000
O2	-2	6h	0.44826	0.03630	1/4	0.0000
O3	-2	6h	0.37289	0.25244	1/4	0.0000
O4	-2	2a	0	0	1/4	0.0000

Table ESI7. Powellite crystallographic unit cell in material HA/MoO (III)

Atom	Ox.	Wyck.	x	y	z
Ca1	+2	4b	0	3/4	3/8
Mo1	+5	4a	0	3/4	7/8
O1	-2	16f	0.12561	0.07210	0.80662

Table ESI8. Powellite crystallographic unit cell in material HA/MoO (IV)

Atom	Ox.	Wyck.	x	y	z
Ca1	+2	4b	0	3/4	3/8
Mo1	+5	4a	0	3/4	7/8
O1	-2	16f	0.10634	0.03192	0.80738

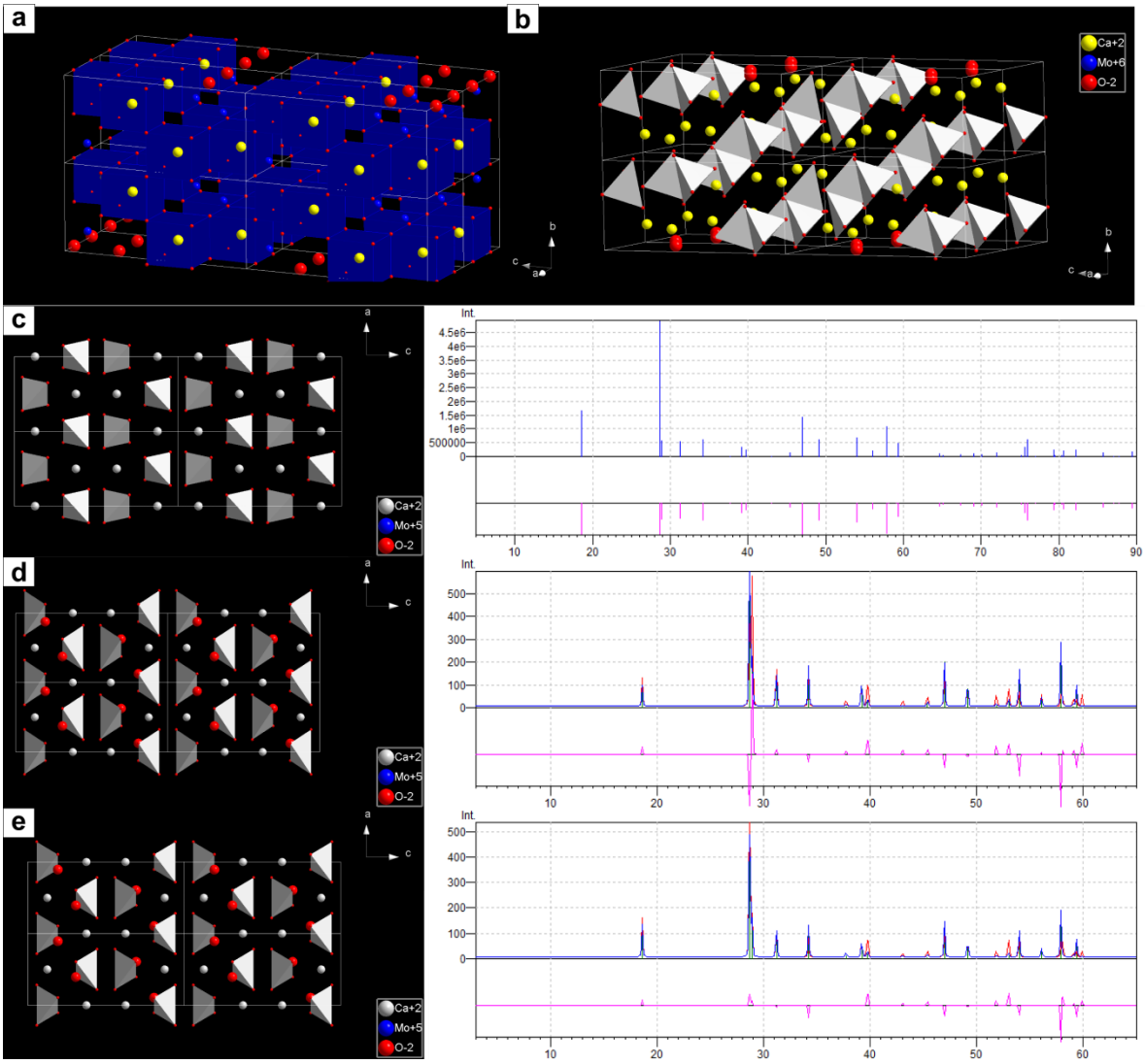

Figure ESI1, Powellite crystallizes in the scheelite structure with the space group I41/a in which the central Ca^{2+} ion is coordinated by eight singly-bound molybdate groups. (a) View of the central Ca^{2+} coordination and (b) of tehaedral MoO_4^{2-} ions in the powellita structure. Comparison of (c) theoretical stoichiometric structure of powellite direct unit cell and modeled analogues for (d) HA/MoO_x (III) and (e) HA/MoO_x (IV) samples; view along crystallographic "*b*" axis. DRX contrast: (blue) theoretical XRD data, (red) experimental XRD data and (pink) match of theoretical and experimental XRD data; total correlation should give a straight line.

ESI-3 Cyclic voltammetry study

Nano-HA/MoOx modified electrodes were prepared as follows: [6] 20.0 mg of each nano-HA/MoO_x sample was dispersed ultrasonically in 1 mL ethanol for 45 min, then 20 μL of the slurry was pipetted and spread on a mirror polished glassy carbon rod (GC, 3 mm diameter), followed by air-drying at room temperature. Afterwards, 10 μL of a Nafion/ethanol solution (0.05 Wt. %) was pipetted on the nano-HA/MoO_x modified-GC electrode. The electrode was left to dry in air for 1 h prior to use.

Electroactive behavior of all materials inspected in this work, were tested against L-Ascorbic acid (AA) redox. L-Ascorbic acid is an essential antioxidant and a cofactor associated with the regulation, development, and maintenance of several cell types in the body, including bones.[6, 7] The activity of AA in living organisms depends on its redox skills, given by the relations among ascorbic acid, semi-dehydroascorbic acid, and dehydroascorbic acid, so it is a recognized redox probe to scrutinize the biological redox status.[8] Expression of heterogeneous rate constant ($k_{(E)}$) for quasi-reversible systems on the positive sweep according to Deakin *et al.* [9],

$$k_{(E)} = D^{1/2} \frac{i}{I_L - I_{(E)}\left(1 + e^{nF/RT(E^{0\prime} - E)}\right)} \quad (7)$$

where i is the current at the time t, I_L is the semi-integral diffusional limiting current, $I_{(E)}$ is the semi-integral current at an applied potential, n is the number of electrons in the rate-determining step, F is the Faraday constant, D is the diffusion coefficient and $E^{o\prime}$ is the formal potential of the two-electron process. For electrochemically irreversible systems, as in the case of AA oxidation, the relationship for the forward wave in the voltammograms is:

$$\ln\left(k_{(E)}\right) = \ln\left(D^{\frac{1}{2}}\right) + ln\left(\frac{i}{I_L - I_{(E)}}\right) \quad (8)$$

All calculations were made with the diffusion coefficient obtained from an electrochemistry handbook. [10] Furthermore, the scan rate dependence with the peak heights for the anodic wave was evaluated by the Randles-Ševčik equation: [11]

$$I_p = 2.687\ x\ 10^5\ An^{3/2}(Dv)^{1/2}C \quad (9)$$

In this expression, I_p is the peak current, A is the electroactive area, C is the concentration of the electroactive specie, n is the number of exchanged electrons, and v is the scan rate, respectively. The rate-determining step (rds) of the reaction could be established by analyzing the slope of the semi-integral CV plot.[12] The transference of a first electron corresponded to a 0.5F/RT slope, where F, R are the Faraday and the gas universal constants respectively and T the absolute temperature. On the other hand, if the transference of the second electron is the rds, the semi-integral CV plot should be associated to a 1.5F/RT slope.[12] The slopes determined from the Randles−Ševčik plots were about 0.48F/RT, indicating that the transference of the first electron is the rds, that is, the formation of the ascorbyl radical anion

ESI-4 Optoelectronic properties

The optical band gap energies (E_g) of polycrystalline HA and nano-HA/MoO_x platforms were estimated from the sharply increasing absorption region according to Tauc and Menth's law [13] extrapolating the adsorption coefficient (α) to zero in the $(\alpha hv)^m$ *vs.* the photon energy (hv) plots.[14] Because only direct allowed transitions are considered, $m = 2$. The adsorption of the sample (A) is converted to the absorption coefficient using the following relationship: [15]

$$\alpha = \left(\frac{2.303\times10^3}{lc}\right) \times A\rho, \quad (10)$$

where ρ is the density of biogenic HA ($\approx 2.23 \pm 0.09$ g cm^{-3}) [16], l is the cuvette length (1 cm), and c is the nanoparticles concentration (1 mg / mL).

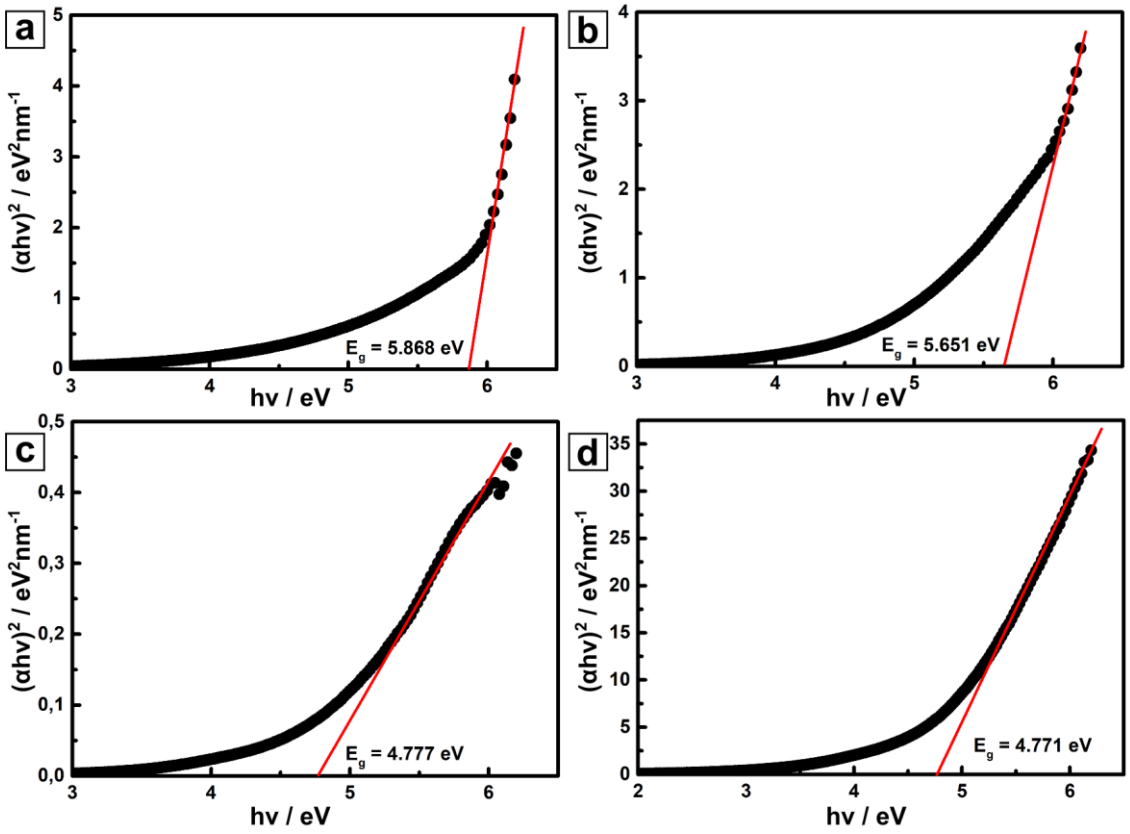

Figure ESI2, optical band gap energy (E_g) of (a) HA, (b) HA/MoOx (II), (c) HA/ MoOx (III) and (d) HA/ MoOx (IV) materials estimated by plotting $(\alpha h\nu)^m$ against the photon energy ($h\nu$).[13]

ESI-5 Biocompatibility assays

Viability of nano-HA and HA/MoOx powders were tested in the presence of calvaria rat osteoblast (rOBs). Primary cultures of rOBs were acquired from calvarias isolated from young Wistar rats as previously described.[17] Animals' care and handling were performed by the animal service of the Department of Biology, Biochemistry and Pharmacy, Universidad Nacional del Sur, Argentina, in agreement with the internationally recognized standard Guide for the Care and Use of Laboratory Animals promulgated by the National Research Council.[18] The active procedures used in this work have been approved by the CICUAE (Institutional Committee for the Care and Use of Experimental Animals, Biology,

Department of Biology, Biochemistry and Pharmacy of the Universidad Nacional del Sur, Argentina). Passage two to four (P2–P4) cells were used.

Materials were autoclaved for 30 min at 120 °C and then PBS dispersion was prepared by placing the components on a rotating mixer for 5 min. Following a 48-well plate was filled with 50 μg/well of sample dispersion and sterilized using UV radiation during 5 h. Finally, the material-coatings were allowed to dry overnight on a shaker in a biological safety cabinet to obtain a homogeneous dry-coat surface on the bottom of the well. Then rOBs were seeded at a density of 10 000 cells per well and cultured for 24 and 48 hs in Alpha-Minimum Essential Medium supplemented with 10% fetal bovine serum (α-MEM-10% FBS, Sigma-Aldrich), in a humidified atmosphere (5.5% CO2) at 37 °C. After treatment, the cell viability estimation was done following the Neutral red uptake assay. [19]

To evaluate the cell morphology and adherence in the presence of the nano-HA and HA/MoOx nanoparticles, the samples were then extended on a microscope slide, air-dried, fixed with absolute ethanol, and stained with Neutral red dye. Experiments were performed with two different cell preparations and repeated five times. Cytomorphometric analysis was done using free Image J (National Institutes of Health, Bethesda, MD) software accordingly to the Foldberg et al. methodology. [20] For the determination of cellular area and its length, each cell was considered an object equivalent to an ellipse, [20] **figure ESI3-b**. Then, the aspect ratio of each cell was estimated by dividing the major axis of the ellipse by the minor. Only cells that were entirely included in the field of vision and exhibited a well-defined cellular and nuclear outlines were selected. The average values of cellular area and diameters of a 20 cells were obtained and recorded. Primary rOBs cultured in absence of material were used as control, C.

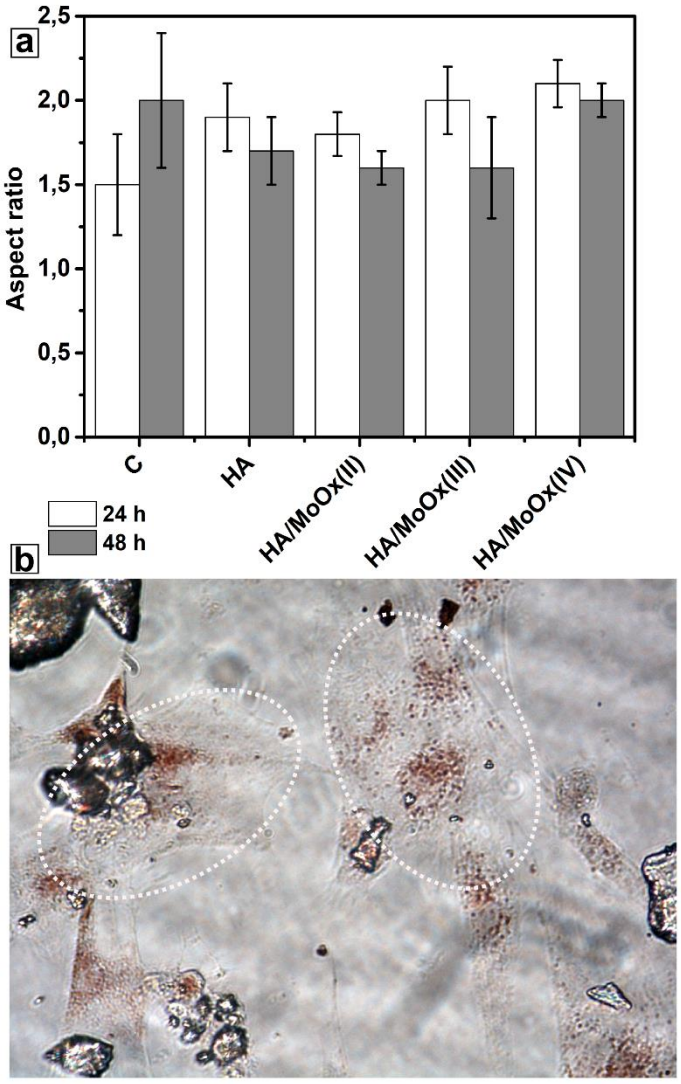

Figure ESI3, **(a)** spreader rat primary osteoblast (rOBs) major to minor axis length ratio after 24 and 48 hrs of culture in the presence of nano-HA/MoOx platforms. **(b)** Elliptical delimitation of the spreader cellular area.

ESI-6 Size distribution histograms of nano-HA and nano-HA/ MoO_x platforms

Size distribution analysis were performed by application of Image J software [21] to FE-SEM microphotographs.

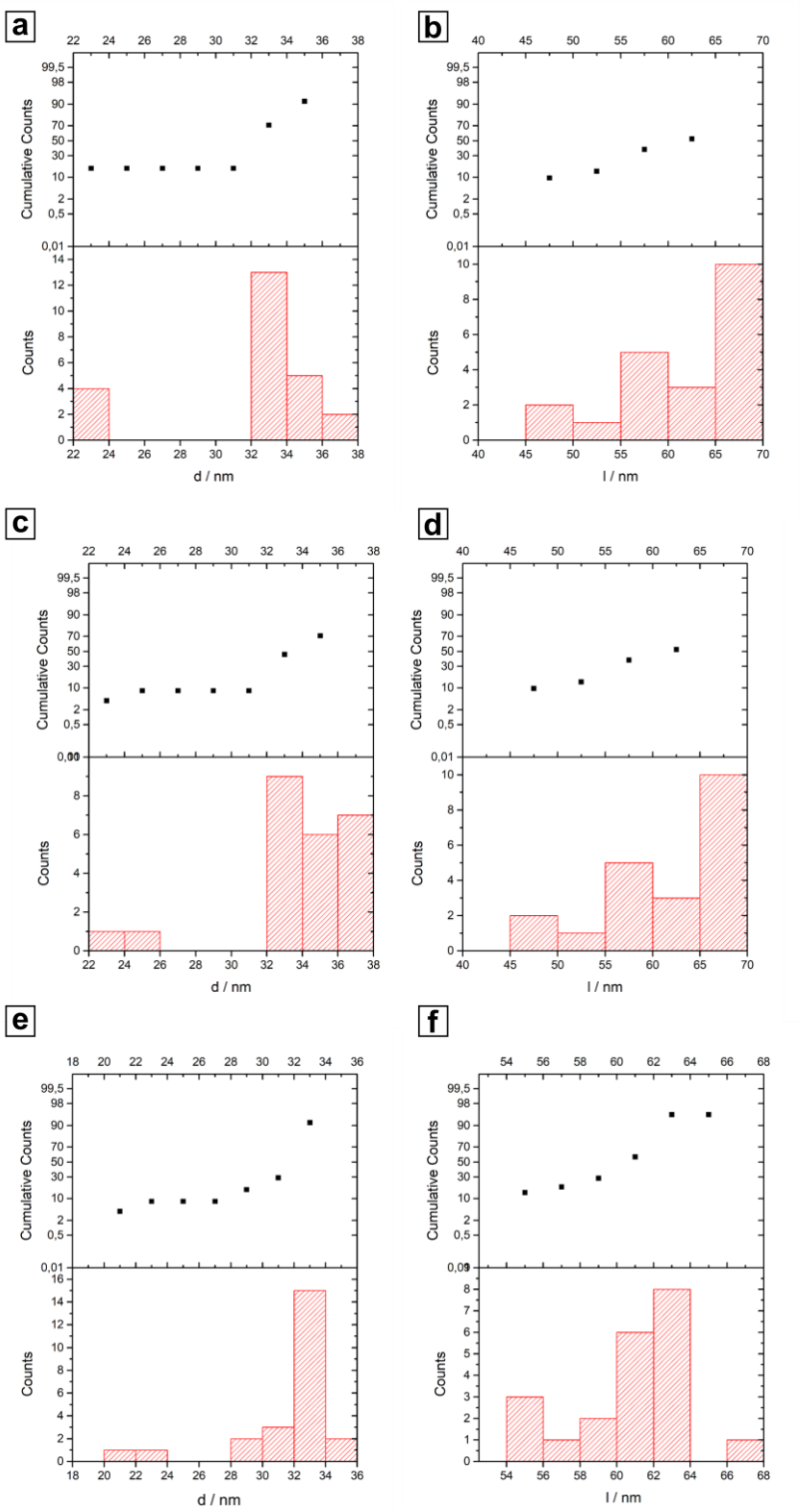

Figure ESI4, diameter (d/ nm) and length (l/ nm) distribution histograms of (a,b) nano-HA, (c,d) nano-HA/ MoO_x (I), (e,f) nano-HA/ MoO_x (II) platforms.

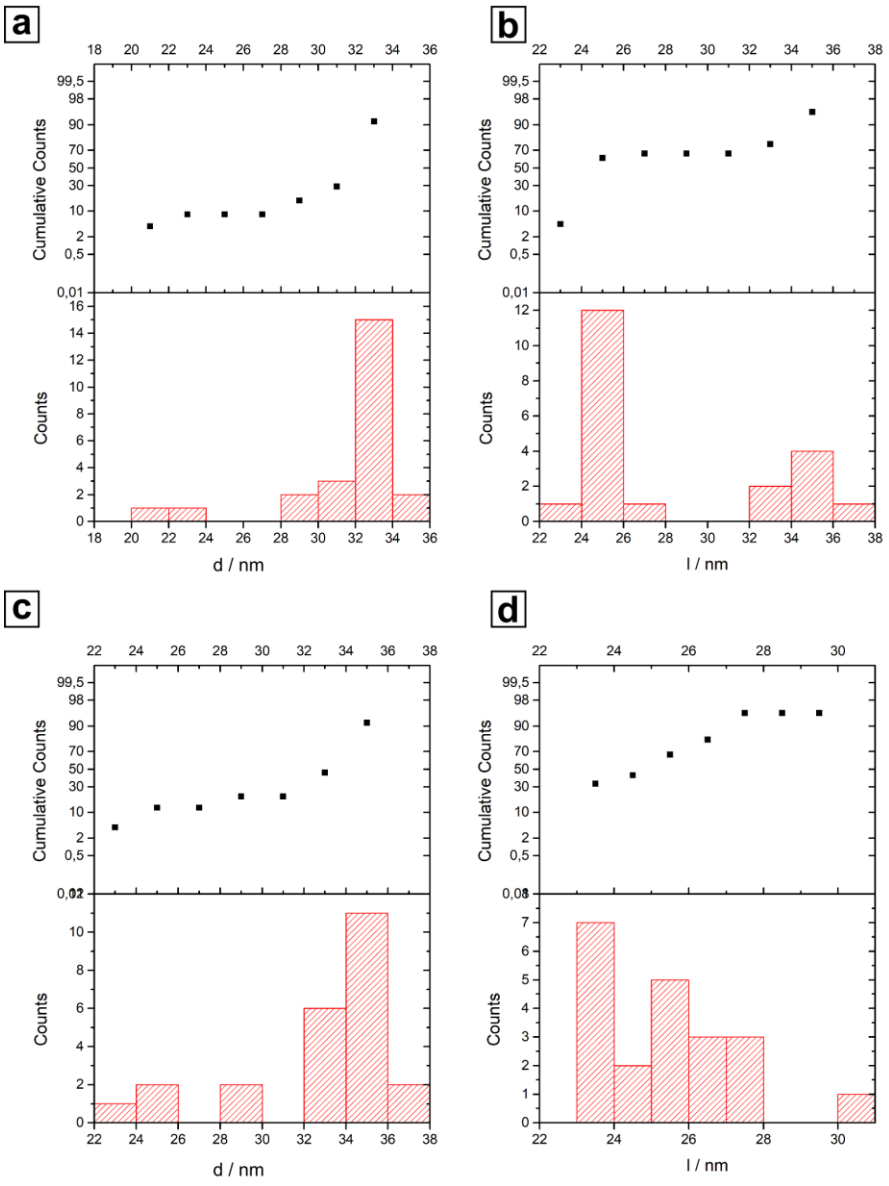

Figure ESI5, diameter (d/ nm) and length (l/ nm) distribution histograms of (a,b) nano-HA/ MoO_x (III) (c,d) nano-HA/ MoO_x (IV) platforms.

Table ESI9, average diameter and length of nano-HA and nano-HA/ MoO_x platforms

Sample	Diameter/ nm	Length /nm
HA	31.8 ± 4.1	60.8 ± 3.9
HA / MoOx (I)	33.4 ± 3.4	60.1 ± 6.4
HA / MoOx (II)	31.3 ± 3.4	60.1 ± 3.1
HA / MoOx (III)	31.5 ± 3.7	27.8 ± 4.6
HA / MoOx (IV)	32.2 ± 3.8	24.9 ± 1.9

ESI-7 Elemental microanalysis

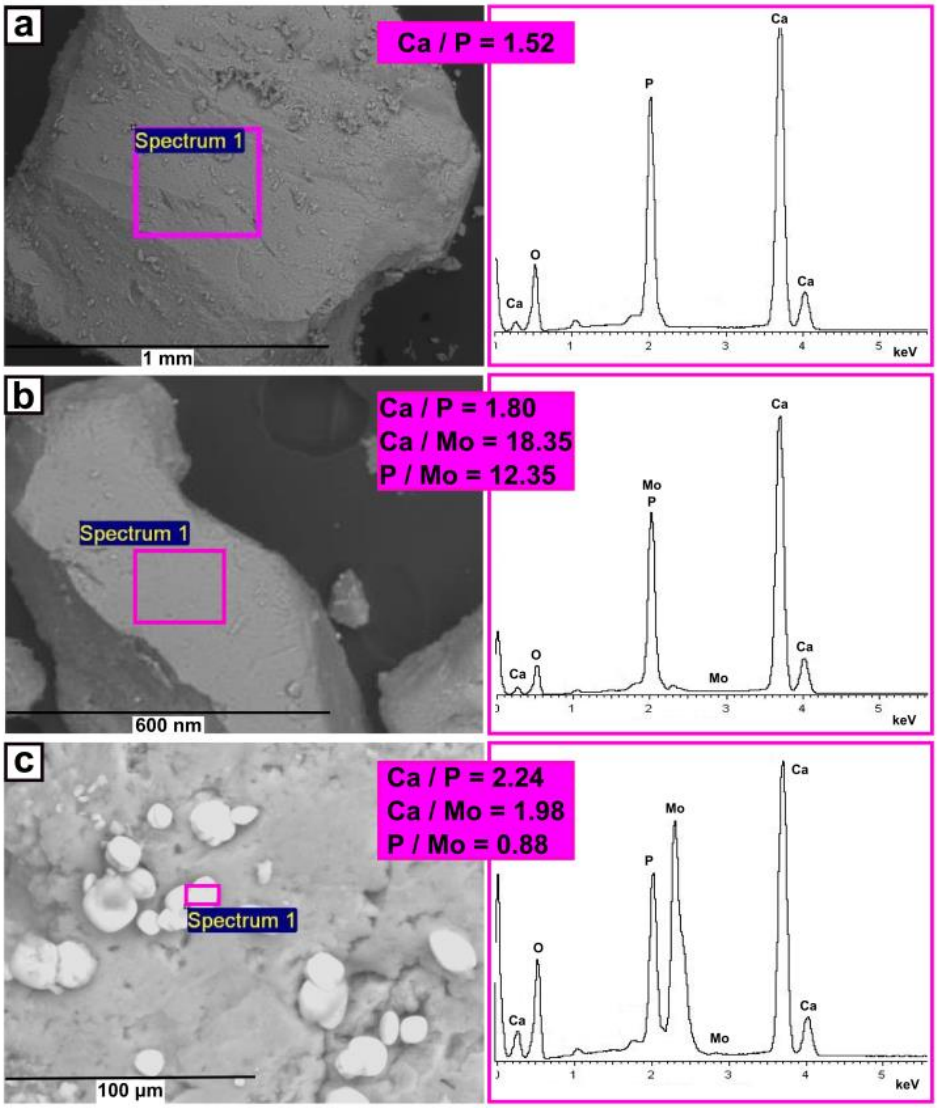

Figure ESI6, EDX microanalysis of (a) un-substituted HA, (b) HA/MoO_x (II) and (c) HA/MoO_x (III) samples.

ESI-8 Nano-HA/MoOx platforms processing

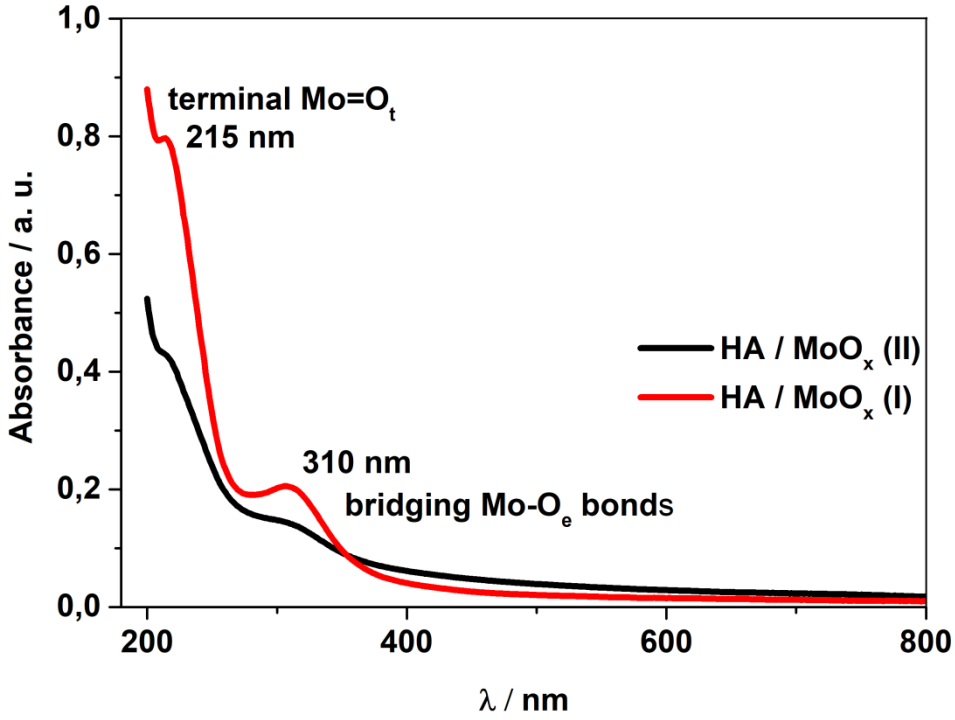

Figure ESI7, UV–vis absorption spectra of the reaction media at the end of the synthesis of HA/MoOx (I) and HA/MoOx (II) samples. Characteristic peaks at 215 and 310 nm are representative of the Keggin heteropolyanions structure. The bands are assigned respectively to the vibrations of terminal Mo=O_t and bridging Mo–O_e bonds. [22]

ESI-9 ξ-potentials measurements

Surface charge of HA and nano-HA/MoO_x platforms were determined at 25.0 ± 0.1 °C using a Malvern Zeta Sizer Nano (ZS90) with a He-Ne laser (633 nm) as a source of incident light, 4 mW max. Experimentally, all samples (0.2 mg / mL) were diluted with filtered hydration medium (PBS, pH = 7.4) to an appropriate counting rate prior to analysis. Reported values were the result of ten independently determinations.

ESI-10 *in Vitro* Hydrolytic Degradation

Each sample was weighted (W_0), 200 mg, and deposited in crystal vessels having 50 mL of PBS (pH = 7.4). Following, they were incubated at 37 ± 0.1 °C throughout 10 days; PBS was refreshed every 3 days. At each time point, samples were collected in triplicate, cleaned carefully with Milli-Q water, blotted with filter paper, and oven-dried until constant weight (W_t). The degradability of nano-HA/MoO_x platforms was computed from the rate of weight loss (% W_L) following the Tampieri et al. methodology [23], results are shown in figure ESI8.

$$\%W_L = \frac{(W_0 - W_t)}{W_0} \times 100 \qquad (11)$$

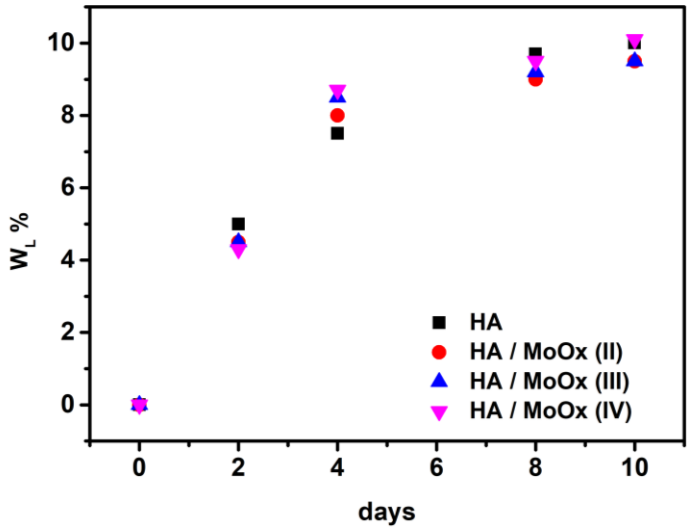

Figure ESI8, Degradation of HA and HA / MoO_x materials at pH = 7.4 and 37 °C.

Supernatant Ca^{2+} concentrations were determined by inductively coupled plasma-atomic emission spectrometry (ICP-AES) using the method 6010C (EPA, 2007). The thermodynamic equilibrium constant of non-stoichiometric HA dissolution, K^0_{sp} was

estimated as $K_{sp}^{0} = (a_{Ca^{+2}})^{10-x}\left(a_{PO_4^{-3}}\right)^{6-x}\left(a_{HPO_4^{-2}}\right)^{x}(a_{OH^-})^{2-x}$, where x is accordingly to elemental microanalysis, section ESI-7. The activities were computed based on the measured concentrations and the Debye–Hückel limiting law: [24]

$$-log(\gamma_i) = AZ_i m^{1/2}\left(1 + Ba_i m^{1/2}\right), \quad (12)$$

where γ_i, a_i, and Z_i are the activity coefficient, the effective diameter, and the valence for species i respectively; $m = \frac{1}{2}\sum_i^n c_i^2 Z_i^2$ is the total ionic strength of the solution; A = 0.51144 and B = $10^{7.515}$ are parameters for the Debye–Hückel limiting law.

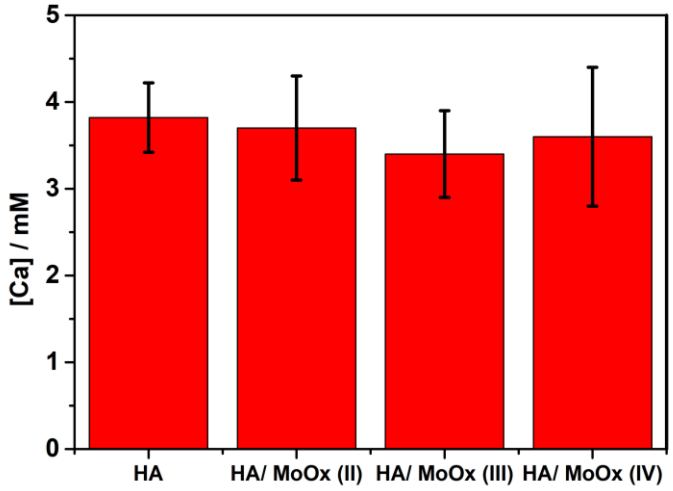

Figure ESI9, Calcium concentration measured after 10 days of material degradation at pH = 7.4 and 37 °C.

As the calcium concentration measured after the degradation of the materials did not present statistically significant differences, we assume that the concentrations of the other ions released from the HA dissolution are also similar. They were calculated according to the solubility product of HA. The MoO_4^{2-} concentration was estimated from the solubility product of powellite for samples HA / MoOx (III-IV); it will be less than

this value in sample HA / MoOx (II) and zero for HA. Obtained values are summarized in **Table ESI10**.

Table ESI10, computed ionic concentration released from samples after 10 days of degradation in PBS (pH = 7.4) at 37°C.

	$[Ca^{2+}]$ / mM	$[PO_4^{3-}]$ /mM	$[HPO_4^{2-}]$ / mM	$[OH^-]$ / mM	$[MoO_4^{2-}]$ / mM
HA	3.82 ± 0.40	2.14 ± 0.22	0.37 ± 0.04	0.47 ± 0.05	0
HA/MoOx (II)	3.70 ± 0.61	2.08 ± 0.21	0.35 ± 0.04	0.45 ± 0.05	< 0.001
HA/MoOx (III)	3.41 ± 0.50	1.91 ± 0.19	0.33 ± 0.04	0.42 ± 0.05	0.001
HA/MoOx (IV)	3.62 ± 0.81	2.03 ± 0.20	0.35 ± 0.04	0.44 ± 0.05	0.001

References

1. B. A. Hunter, Rietica - a visual Rietveld program, Australia, 2000.
2. R. J. Tilley, *Crystals and crystal structures*, John Wiley & Sons, 2006.
3. S. K. Padmanabhan, A. Balakrishnan, M.-C. Chu, Y. J. Lee, T. N. Kim and S.-J. Cho, *Particulology*, 2009, **7**, 466-470.
4. E. Bouyer, F. Gitzhofer and M. Boulos, *J. Mater. Sci.: Mater. Med.*, 2000, **11**, 523-531.
5. I. Cacciotti, A. Bianco, M. Lombardi and L. Montanaro, J. Eur. Ceram. Soc., 2009, **29**, 2969-2978.
6. N. C. Andrés, J. M. Sieben, M. Baldini, C. H. Rodríguez, Á. Famiglietti and P. V. Messina, *ACS Appl. Mater. Interfaces*, 2018, **10**, 19534-19544.
7. P. Aghajanian, S. Hall, M. D. Wongworawat and S. Mohan, *J. Bone Miner. Res.*, 2015, **30**, 1945-1955.
8. S. E. Bohndiek, M. I. Kettunen, D.-e. Hu, B. W. Kennedy, J. Boren, F. A. Gallagher and K. M. Brindle, *J. Am. Chem. Soc.*, 2011, **133**, 11795-11801.
9. M. R. Deakin, P. M. Kovach, K. J. Stutts and R. M. Wightman, *Anal. Chem.*, 1986, **58**, 1474-1480.
10. C. G. Zoski, *Handbook of electrochemistry*, Elsevier, 2006.
11. A. J. Bard and L. R. Faulkner, *Electrochemical Methods: Fundamentals and Applications*, John Wiley, 2001.
12. I. F. Hu and T. Kuwana, *Anal. Chem.*, 1986, **58**, 3235-3239.
13. J. Tauc and A. Menth, J. Non-Cryst. Solids, 1972, **8**, 569-585.
14. J. M. Ruso, V. Pardo, J. Sartuqui, N. Gravina, N. L. D'Elía, O. I. Pieroni and P. V. Messina, *ACS Appl. Mater. Interfaces*, 2015, **7**, 12740-12750.
15. N. Serpone, D. Lawless and R. Khairutdinov, *J. Phys. Chem.*, 1995, **99**, 16646-16654.
16. B. He, S. Huang, J. Jing and Y. Hao, *Arch. Oral Biol.,* 2010, **55**, 134-141.
17. N. L. D'Elía, A. N. Gravina, J. M. Ruso, J. A. Laiuppa, G. E. Santillán and P. V. Messina, *Biochim. Biophys. Acta, Gen. Subj.*, 2013, **1830**, 5014-5026.

18. National, Research and Council, *Guide for the care and use of laboratory animals*, National Academies Press, 2010.
19. G. Repetto, A. del Peso and J. L. Zurita, *Nat. Protoc.*, 2008, **3**, 1125.
20. S. Foldberg, M. Petersen, P. Fojan, L. Gurevich, T. Fink, C. P. Pennisi and V. Zachar, *Colloids Surf., B,* 2012, **93**, 92-99.
21. C. A. Schneider, W. S. Rasband and K. W. Eliceiri, *Nat. Methods*, 2012, **9**, 671.
22. J. Javidi, M. Esmaeilpour, Z. Rahiminezhad and F. N. Dodeji, *J. Cluster Sci.*, 2014, **25**, 1511-1524.
23. A. Tampieri, M. Iafisco, M. Sandri, S. Panseri, C. Cunha, S. Sprio, E. Savini, M. Uhlarz and T. Herrmannsdörfer, *ACS Appl. Mater. Interfaces*, 2014, **6**, 15697-15707.
24. E. Huckel and P. Debye, *Phys. Zeitschrift*, 1923, **24**, 185.